Check for updates

Controllable fabrication of a hybrid containing dodecyl dihydrogen phosphate modified magnesium borate whisker/hydrated alumina for enhancing the fire safety and mechanical properties of epoxy resin†

Sai Zou,‡[a] Shengjie Lan,‡[ab] Li Dang,[a] Ping Li,[a] Donghai Zhu [ID] *[a] and Le Li[a]

A composite particle with hydrated alumina deposited on the surface of magnesium borate whisker (MBW@HA) was prepared following a chemical liquid deposition method. Subsequently, dodecyl dihydrogen phosphate (DDP) was grafted onto the surface of the composite particles to synthesize an inorganic–organic hybrid (MBW@HA–DDP). The structure, morphology, and composition of MBW@HA–DDP were well characterized. The results revealed the hybrid of MBW@HA–DDP was successfully synthesized characterized by a hydrophobic surface. Subsequently, the obtained MBW@HA–DDP was incorporated into epoxy resin (EP) to fabricate flame retardant composites. The results revealed that the incorporation of MBW@HA–DDP significantly improved the fire safety of EP, for instance, the total heat release (THR) and peak heat release rate (PHRR) of the EP composite with 10-phr MBW@HA–DDP added were reduced by 28.1% and 32.0%, respectively, accompanied with lower total smoke production (TSP) and smoke production rate (SPR). The improved fire safety was due to the barrier function of MBW and HA, and the dilution effect of water vapor generated from HA. Meanwhile, the phosphorus oxoacids generated from DDP could function as catalysts and increase the degree of graphitization of the char residues, thus protecting the matrix effectively. In relation to mechanical properties, the incorporation of MBW@HA–DDP did not deteriorate the mechanical properties of EP but improved them to some extent. The results presented herein help develop a novel strategy for developing flame retardants characterized by good flame-retardant behavior and improved mechanical properties.

1. Introduction

Epoxy resin (EP) is an excellent thermosetting resin material with good dimensional stability, corrosion resistance, heat resistance, electrical insulation, and low curing shrinkage. It is widely used in the adhesives, coatings, composites, and construction engineering fields.[1–3] However, this kind of material is highly flammable. EP burns following ignition, resulting in the production of smoke, harmful gases, and molten droplets.[4–6] Thus, the risk of catching fire increases, and this endangers the lives of people and the environment. Therefore, developing new flame retardants with good smoke suppression performance and high flame retarding efficiency is imperative for the application of EP.

In general, flame retardants can be divided into reactive and additive flame retardants according to whether they form chemical bonds with the polymer matrix. The additive flame retardant is introduced into the matrix following the process of physical blending. Unlike the reactive flame retardant, the additive flame retardant is easy to use, can be easily fabricated, and is cost-effective.[7,8] Hydrated alumina (HA) is classified as an additive flame retardant and is widely used in the industry because of its low cost, no pollution, no halogens, and smoke suppression.[9,10] However, owing to their strong hydrophilic and the existence of hydrogen bond force, HA particles are liable to re-aggregate, and hence it is difficult to disperse them evenly on a hydrophobic polymer matrix. Furthermore, efficient flame suppression can be achieved under high HA loading conditions when only HA is used as the additive. Under these conditions, the mechanical properties of the polymer composites deteriorate.[11,12] To address these issues, many researchers concentrated on modifying the surface of HA using silane coupling agents, stearic acid, or titanate coupling agents. The results reveal that surface

[a]State Key Laboratory of Plateau Ecology and Agriculture, School of Chemical Engineering, Qinghai University, Xining 810016, PR China. E-mail: zhudonghai-2001@163.com

[b]Qinghai Institute of Salt Lakes, Chinese Academy of Sciences, Xining 810008, PR China

† Electronic supplementary information (ESI) available. See DOI: 10.1039/d1ra08289b

‡ Sai Zou and Shengjie Lan contributed equally to this work.

modification of HA can not only improve the extent of dispersion in the polymer matrix but also help increase the degree of interface adhesion between HA and the polymer matrix.[13,14] However, there is no enhancement effect of HA, and the process of surface modification alone cannot fundamentally address the issue of degraded mechanical properties of polymer composites.
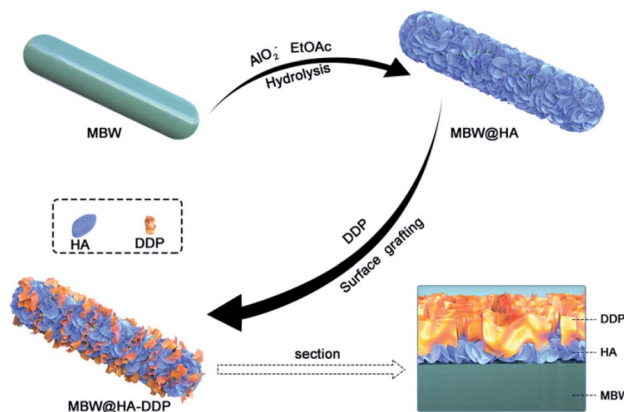
In recent years, polymers reinforced with fibers of synthetic or natural materials have gained extensive attention in both areas of engineering and research technology. Fibers (such as glass, carbon, sisal, *etc.*) primarily play the role of skeleton support in polymer composites, and exhibit excellent strengthening effects in polymer matrix.[15–19] Magnesium borate whisker (MBW) is a short fiber derived from natural minerals. It can also be produced following the process of chemical synthesis.[20–23] According to previous reports, the mechanical properties of polymers can be improved by embedding MBW into them. The improvement can be primarily attributed to the near-perfect crystal structure and high tensile strength of the composites.[24–27] Moreover, several studies show that the incorporation of the combination of fiber and flame retardant with good flame retardant performance could simultaneously enhance the flame retardancy and mechanical properties of EP.[28–30] For this reason, MBW were selected by us to treat EP composites to address the problem of the degradation of mechanical properties in the presence of HA. To our knowledge, there's no work has been reported on the controllable fabrication of HA shell on the surface of MBW. The process results in the fabrication of MBW@HA composite particles that help improve the mechanical properties and fire safety of EP. In addition, to achieve better dispersion of the MBW@HA composite particles in the EP matrix and improved flame retardancy, dodecyl dihydrogen phosphate (DDP) was used as the surface graft agent (as chemical bonds could be formed between the –OH groups present on the surface of the MBW@HA composite particles and the P=O–OH group present in DDP) and the flame retardant synergist.[31,32] The alkyl chain in DDP was compatible with the EP matrix. DDP contains phosphorus and follows a different mechanism to achieve flame retardancy in the presence of HA.[33–35] This indicates the generation of good synergistic effects between them on flame retardant EP.

In this work, MBW@HA composite particles were prepared by the chemical liquid deposition method. Following this, DDP was grafted onto the surface of MBW@HA to synthesize an inorganic–organic hybrid (MBW@HA–DDP). The synthetic scheme is shown in Scheme 1. The structure, morphology, and composition of MBW@HA–DDP were determined. Afterwards, the hybrid of MBW@HA–DDP was mixed with EP to prepare the polymer composites. The mechanical properties, smoke suppression and flame retardancy effect of MBW@HA–DDP on EP were investigated, and the mechanism of action was analyzed.

2. Experimental

2.1. Materials

Magnesium borate whisker (MBW) was prepared in our laboratory following a combination of the co-precipitation and calcination processes. We have previously reported the detailed

Scheme 1 Synthetic route of MBW@HA–DDP inorganic–organic hybrid.

procedure.[36] Sodium aluminate (NaAlO$_2$, AR), ethyl acetate (EtOAc, AR), dodecyl dihydrogen phosphate (DDP, AR), and absolute ethanol (AR) were purchased from Aladdin Biochemical Technology Co., Ltd. (Shanghai, China). Epoxy (EP, E-44) was provided by Nantong Xingchen Co., Ltd. (Jiangsu, China). 4,4-Diaminodiphenyl methane (DDM, AR) was purchased from Sinopharm Chemical Reagent Co., Ltd. (Shanghai, China).

2.2. Preparation of MBW@HA and MBW@HA–DDP

NaAlO$_2$ (2.65 g) was dissolved completely in 200 mL of distilled water under conditions of continuous stirring on a magnetic stirrer at 60 °C. Following this, MBW (10.00 g) was added to the previously prepared solution and ultrasonically dispersed for 20 min. Subsequently, 10 mL of EtOAc was added dropwise into the prepared suspension, and the mixture was stirred at 60 °C for 2 h. Afterwards, the slurry was filtered, washed several times with absolute ethanol and distilled water. Finally, the sample was dried at 100 °C over a period of 12 h to obtain MBW@HA. HA was prepared following a similar procedure under the same conditions.

The obtained MBW@HA (10.00 g) was dispersed in distilled water (200 mL) under conditions of sonication. Following this, 0.55 g of DDP was dissolved in 20 mL of absolute ethanol, and the solution of DPP was added dropwise at 60 °C into the previously prepared slurry following which the solution was vigorously stirred for 1 h. Following the completion of the reaction, the product was filtered, washed with absolute ethanol and distilled water. The sample was then freeze-dried over 12 h to obtain MBW@HA–DDP.

2.3. Preparation of EP composites

EP composites containing various fillers were prepared following a melt-mixing method. The formulations used for preparing the various EP composites are presented in Table 1. EP exhibited good fluidity when heated at 90 °C. Various fillers were incorporated separately to melt EP under conditions of constant stirring (stirring time: 2 h). Different fillers were used to produce different sets of EP samples. Subsequently, a curing

agent (DDM) was added to the above system, and the mixture was continuously stirred until the curing agent dissolved completely. The formed mixture was put in a vacuum drying oven heated at 90 °C and heated for several minutes under conditions of vacuum to remove residual bubbles. Finally, it was poured into stainless steel molds and cured at 100 °C for 2 h. Following this, the temperature was raised to 150 °C and the sample was heated at this temperature for 2 h. Following the curing process, all samples were allowed to cool naturally to room temperature. A pure EP sample was prepared following a similar procedure in the absence of fillers.

2.4. Characterization

The SEM images were recorded using a JSM 6700 field emission scanning electron microscope (JEOL, Japan) to observe the morphologies of the synthetic products and their dispersion states in the EP matrix. Water contact angle (WCA) was measured using a DSA30 digital goniometer (Kruss, Germany). The energy-dispersive X-ray spectroscopy (EDS) technique was used for elemental mapping, and the process was conducted on a JEOL 2010 (JEOL, Japan) system under the scanning TEM in EDS mode. X-ray diffraction (XRD) patterns were recorded using a Siemens D5000 X-ray diffractometer (Karlsruhe, Germany) equipped with Cu Kα radiation ($\lambda = 0.1542$ nm). Fourier transform infrared (FTIR) spectra were recorded on an AVATAR 360 FTIR spectrometer (Thermo Nicolet Corp., USA). The cone calorimeter test (CCT, Modisco Combustion Technology Instrument Co., Ltd., China) was conducted to determine the fire performance of the EP composites according to ISO 5660. The sample dimensions were $100 \times 100 \times 3$ mm^3, and the experiments were conducted when the heat flux was 50 kW m^{-2}. Tensile properties were tested using an HD 021NS-5 tensile tester (Nantong Hongda experimental instrument Co., Nantong, China) according to ASTM D638. The sample dimensions were $165 \times 13 \times 3$ mm^3. The impact strength was measured in accordance with ASTM D256 using a 501J-4 digital impact test machine (Shenzhen Wance Testing Machine Co. Ltd., China). The Raman spectroscopy data for residual char were collected using an RM2000 Raman spectrometer (Renishaw, UK) equipped with an Argon ion laser as the light source (wavelength = 532 nm). The X-ray photoelectron spectroscopy (XPS) technique was also used to analyze the samples, and the experiments were conducted on an Escalab 250 Xi spectrometer (Thermofisher, American) (Al Kα X-ray source; 1486.6 eV). Thermogravimetric analysis (TGA) was conducted using a Netzsch STA449F3

analyzer (Netzsch, Germany) from 20 °C to 800 °C with a heating rate of 10 °C min^{-1} under N$_2$ atmosphere.

3. Results and discussion

3.1. Characterization of the as-prepared samples

The morphologies and structures of the as-prepared samples were examined using the SEM and TEM. The WCA values were also determined. The naked MBW exhibited a typical rod structure characterized by a clean and smooth surface (Fig. 1a). Fig. 1b shows that the HA obtained following the hydrolysis of NaAlO$_2$ were spherical grain-like agglomerates. The agglomerate could be attributed to the presence of hydrogen bonds and other strong polar forces among HA particles. It was observed that the surface of the alumina-coated MBW (MBW@HA, Fig. 1c) was rough and covered with interconnected primary nanoflakes that resembled small anchor flukes, which could be easily embedded into the EP matrix.[37] The morphology of MBW@HA–DDP (Fig. 1d) was similar to that of the MBW@HA sample. It is noteworthy that the surface properties of the two samples were significantly different from each other (reflected by the WCA values; upper right corner of Fig. 1c and d). The WCA increased from 0° to approximately 120° following the process of DDP modification, indicating that MBW@HA–DDP was hydrophobic and exhibited good binding affinities toward the EP matrix. The results obtained from TEM elemental mapping tests conducted with MBW@HA–DDP revealed that Al, C, and P were distributed uniformly on MBW. Based on these findings, it was hypothesized that the surface of MBW was coated with HA, followed by the introduction of DDP.

The XRD patterns recorded for MBW, HA, MBW@HA, and MBW@HA–DDP (Fig. 2) were analyzed to study the structural features of the as-fabricated samples. It was observed that the characteristic peaks of monoclinic Mg$_2$B$_2$O$_5$ appeared at 19.91°, 29.95°, 31.71°, 35.06°, 45.11°, and 47.35° (PDF card 86-0531) for MBW (Fig. 2a).[38] The XRD pattern of HA (Fig. 2b) obtained following the hydrolysis of NaAlO$_2$ does not show any diffraction peaks of crystal alumina.[39] Thus, the XRD patterns of MBW@HA only show the diffraction peaks of MBW (Fig. 2c). In addition, the diffraction peaks recorded for the MBW@HA–DDP sample were similar to the diffraction peaks recorded for the MBW@HA sample. However, the relative intensities of the diffraction peaks decreased under these conditions, suggesting that the surface of MBW@HA was enclosed by DDP. The results also indicated that it was poorly crystallized.

Table 1 Formulations of pure EP and its composites

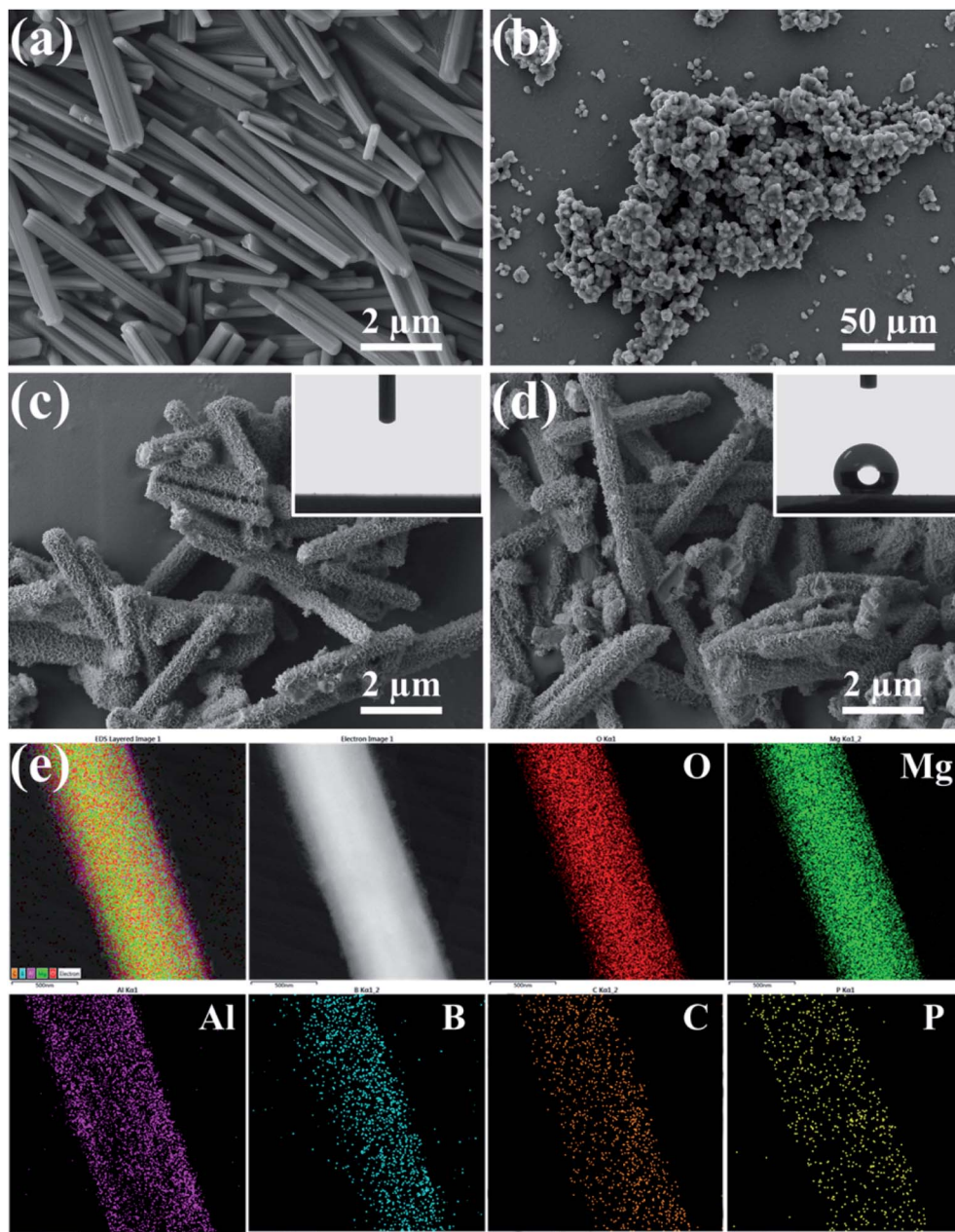| Sample	EP (phr)	DDM (phr)	HA (phr)	MBW (phr)	MBW@HA (phr)	MBW@HA–DDP (phr)
EP	100	22	0	0	0	0
EP1	100	22	10	0	0	0
EP2	100	22	0	10	0	0
EP3	100	22	0	0	10	0
EP4	100	22	0	0	0	10

Fig. 1 SEM images of (a) MBW, (b) HA, (c) MBW@HA, and (d) MBW@HA–DDP. (e) TEM images of MBW@HA–DDP and the results of the corresponding elemental mapping analyses of O, Mg, Al, B, C, and P.

FTIR spectra were also recorded to further understand the structure of the as-synthesized samples. As shown in Fig. 3b, the FTIR spectral profiles recorded for HA, obtained following the hydrolysis of $NaAlO_2$, reveal the presence of stretching vibration bands corresponding to the O–H groups at 3620 cm^{-1}, 3525 cm^{-1}, 3457 cm^{-1}, and 3384 cm^{-1}. The band at 1021 cm^{-1} corresponds to the vibration of Al–O.[40] This result agrees well with the result obtained by analyzing the standard spectral profile of $Al(OH)_3$. In addition to the typical bands corresponding to MBW, the characteristic bands of HA were also present in the spectral profile recorded for the MBW@HA sample (Fig. 3c). This indicated that HA was successfully coated

onto the surface of MBW. Two absorption bands, attributable to the asymmetric and symmetric stretching vibrations of CH_2, were observed in the spectral profiles recorded for the MBW@HA–DDP sample at 2922 cm^{-1} and 2850 cm^{-1} (Fig. 3d). These bands were absent in the profile recorded for the MBW@HA sample. Furthermore, the intensity of the four absorption bands assigned to the O–H groups decreased following the process of DDP modification. This indicated the successful grafting of DDP onto the surface of MBW@HA via chemical bonding.[41] The deformation vibration band corresponding to CH_2 (at 1468 cm^{-1}) and the P–O–C stretching vibration band (at approximately 1030 cm^{-1}) could not be
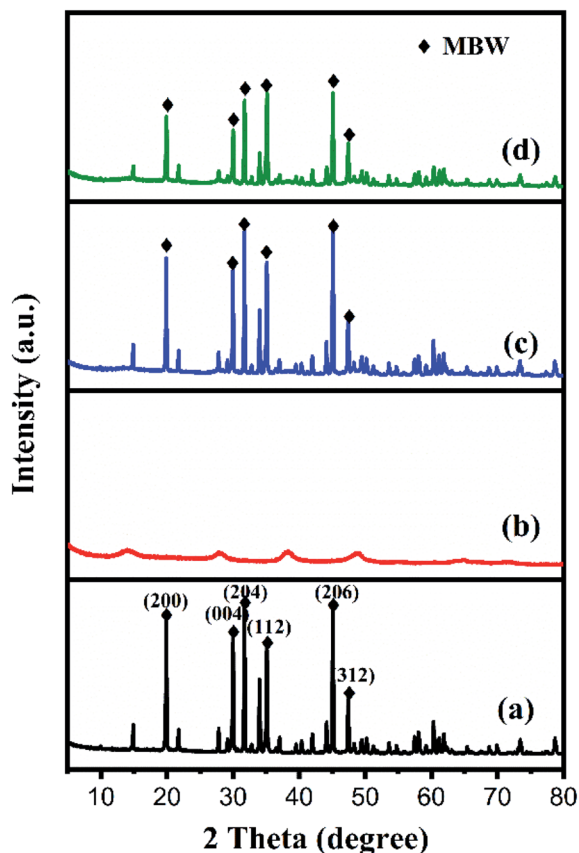
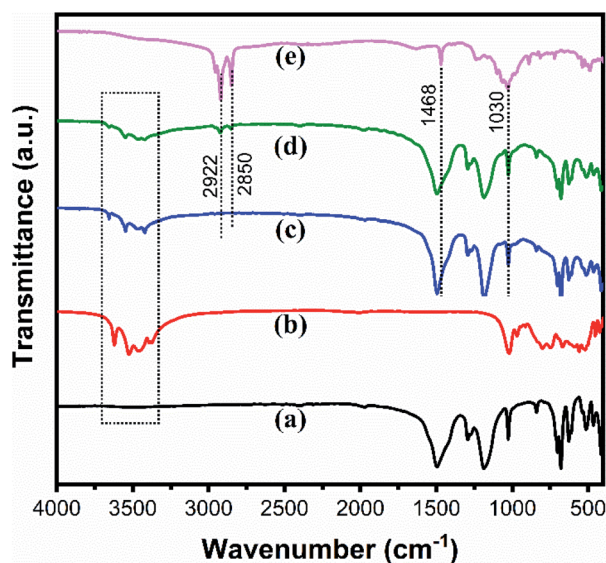Fig. 2 XRD patterns recorded for (a) MBW, (b) HA, (c) MBW@HA, and (d) MBW@HA–DDP.

Fig. 3 FTIR spectral profiles recorded for (a) MBW, (b) HA, (c) MBW@HA, (d) MBW@HA–DDP, and (e) DDP.

identified in the spectral profile recorded for the MBW@HA–DDP sample. This could be attributed to the presence of the highly intense strong bands corresponding to the boron-containing functional groups.

The composition of MBW@HA–DDP was determined by thermogravimetric analysis (TGA). The specific results were shown in Fig. S1 and Table S1.† Before 800 °C, MBW was very stable and hardly decomposed. In contrast, HA and MBW@HA present residual weight percentages of 64.61 and 93.64% at 800 °C. Then, it can be calculated that the MBW and HA weight percentages for MBW@HA are 82.03 and 17.97%, respectively. Regarding MBW@HA–DDP, there was a clearly weight loss step range of 200–480 °C in comparison with that of MBW@HA. This was due to the combustion of DDP and it normally burns off after 480 °C. Thus, the weight percentage of MBO, HA, and DDP in the MBW@HA–DDP hybrid was 78.00, 17.09, and 4.91%, respectively.

3.2. Mechanical properties of the EP composites

The mechanical properties of the composites are a crucial factor for their practical applications. In this work, the tensile strength and impact strength of pure EP and its composites were studied. The test results are presented in Fig. 4. Compared to pure EP, both of the tensile strength and impact strength of EP1 were reduced significantly following the addition of 10 phr of HA. This mainly because that the HA particles could easily agglomerate inside the EP matrix as they were characterized by large specific surface areas and high polarity. Surprisingly, the impact strength and tensile strength of EP2 remained lower than those of pure EP, following the addition of 10 phr of naked MBW. This indicated that MBW played little role in improving the properties of untreated EP. When MBW was replaced with the same amount of MBW@HA, the tensile strength of EP3 was clearly improved, although its impact strength was still worse than pure EP. When the same amount of MBW@HA–DDP was incorporated to the EP matrix, the impact strength and tensile strength of EP4 increased to 10.6 kJ m^{-2} and 74.2 MPa, respectively. The values were higher than the values recorded for pure EP.

The tensile fracture surfaces of EP, EP1, EP2, EP3, and EP4 were observed using the SEM technique to further study the
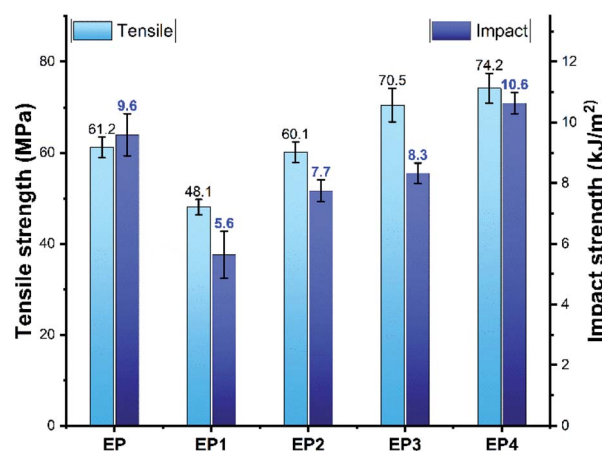

Fig. 4 Tensile strength and impact strength of pure EP and its composites.

reinforcing effect of the MBW@HA–DDP sample on EP. As shown in Fig. 5c, the naked MBW were unevenly scattered in EP2, acting as the initiating flaws and resulting in poor mechanical properties. Similar results were observed for EP3 (Fig. 5d). Some of the MBW@HA rods were pulled out or detached from the EP matrix. This indicated poor interfacial compatibility between the participants. The surface of the MBW@HA rod was rougher than the surface of the naked MBW. The former is characterized by a multilevel structure, which could be easily embedded into the EP matrix. Thus, the mechanical properties of EP3 were better than those of EP2. The MBW@HA–DDP rods in EP4 (Fig. 5e) were tightly bound to the EP matrix. Gaps were absent, indicating that DDP modification resulted in significantly improved interfacial compatibility. The presence of some broken MBW@HA–DDP rods was observed on the tensile fracture surfaces of EP4, indicating the transfer of stress. Thus, the mechanical properties of EP4 can be further improved.

3.3. Flame retardancy of EP composites

Cone calorimeter test (CCT) was employed to assess the flame retardancy of EP composites, as it can reflect a burning scenario resembling a real fire. The total heat release (THR) and heat release rate (HRR) curves generated for the samples are illustrated in Fig. 6, and the detailed values are summarized in Table 2. For pure EP, the THR and peak of HRR (PHRR) values could reach 110.0 MJ m^{-2} and 1262.6 kW m^{-2}, respectively, indicating that it burns vigorously when ignited. For EP1, After the addition of 10-phr HA obtained by hydrolysis of NaAlO$_2$, the THR and PHRR values were reduced by 19.2% and 24.7%, respectively, in contrast to pure EP. This could be attributed to the endothermic decomposition reaction of HA. The water vapor and Al$_2$O$_3$ produced during the decomposition processes of HA can be used to dilute and

isolate oxygen and flammable gases. Compared with pure EP, by the presence of 10-phr the naked MBW, the THR and PHRR values of EP2 were reduced by 11.5% and 13.8%, respectively. This can be primarily ascribed to the barrier effect of MBW. When the amount of MBW@HA–DDP introduced into the EP matrix was the same as that of MBW@HA, a further reduction in the THR and PHRR values of the composites was observed. As a result, compared with pure EP, the THR and PHRR values of EP4 were reduced by 28.1% and 32.0%, respectively. The flame retardancy effect of MBW@HA–DDP on EP was also compared with those of metal hydroxides such as magnesium hydroxide (MH) and layered double hydroxide (LDH) that are commonly used to meliorate the flame retardant properties of polymers. As shown in Table S2,† the PHRR and THR of EP composite with MBW@HA–DDP added were reduced to a greater degree than with the same amount of MH or LDH added, showing that MBW@HA–DDP has better flame retardancy. In addition, the incorporation of MBW@HA–DDP did not deteriorate the mechanical properties of EP but improved it to some extent.

As shown in Table 2, the incorporation of different samples can result in an increase in the rate of formation of char residues for all the EP composites. The increases varied by different degrees under conditions of the same burning time. Especially, the char residue rate recorded for EP4, containing 10-phr MBW@HA–DDP, was the highest, reaching 23.4%. The results indicated that the introduction of DDP could further enhance the flame retardancy of the composites. On the one hand, DDP contributes to the formation of a compact carbon layer, which effectively inhibits the further combustion of the EP composites during the process of combustion when the dehydrated product is formed under conditions of catalysis.[41] On the other hand, the newly formed HO˙ and H˙ radicals during the combustion of EP could be trapped by the PO˙ radical generated from DDP.[42,43] This can prevent the spread of fire.
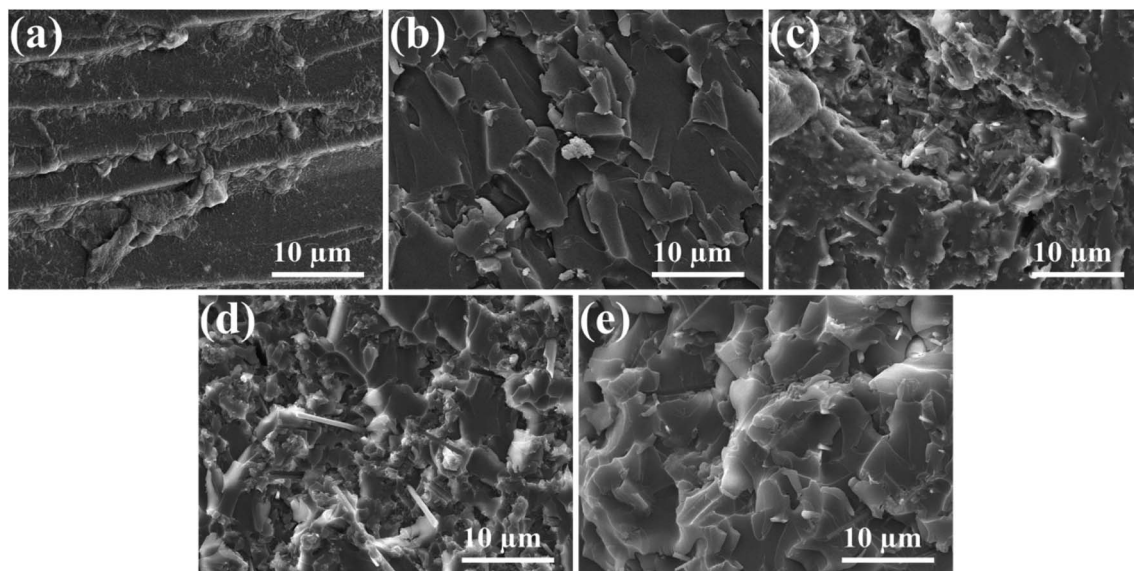

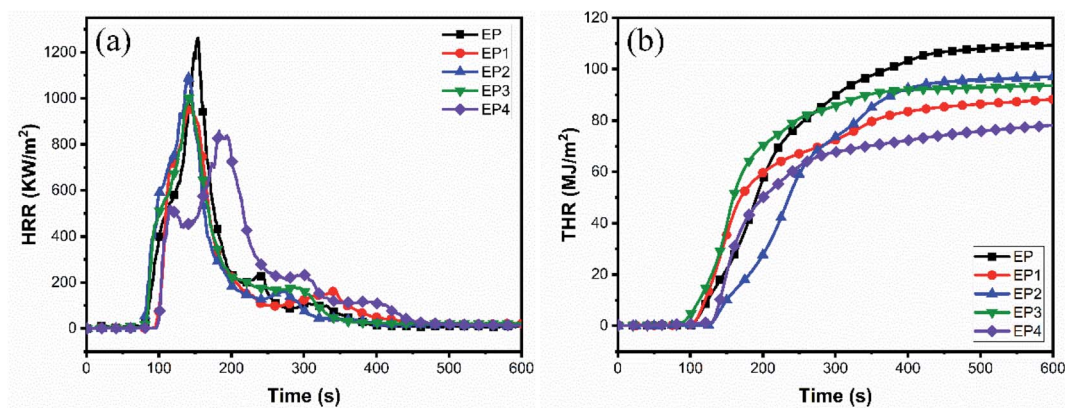Fig. 5 SEM images of the fracture surfaces of (a) EP, (b) EP1, (c) EP2, (d) EP3, and (e) EP4.

Fig. 6 (a) HRR and (b) THR curves generated for pure EP and its composites.

Table 2 CCT data recorded for pure EP and its composites

Sample	PHRR (kW m^{-2})	THR (MJ m^{-2})	Char residue (%)	SPR (m^2 s^{-1})	TSP (m^2)
EP	1262.6	110	13.1	0.55	85.5
EP1	950.6	88.9	18.6	0.36	40.5
EP2	1088.2	97.3	19.3	0.46	67.5
EP3	1014.7	93.9	21.0	0.44	48.9
EP4	858.6	79.1	23.4	0.32	43.0

3.4. Smoke suppression achieved using EP composites

The results obtained from CCT can also be used to assess the smoke suppression effect generated by different fillers by measuring the total smoke produced (TSP) and smoke production rate (SPR) for the EP composites. Analysis of the peak SPR (PSPR) value recorded for pure EP was as high as 0.55 m^2 s^{-1}, suggesting that a large amount of smoke could be produced during the process of combustion (Fig. 7 and Table 2). The addition of 10 phr of HA into the EP matrix can effectively decrease the PSPR value of the composite, which is 34.5% lower than the value recorded for pure EP. This can be primarily attributed to the adsorption effect and the physical barrier effect of Al$_2$O$_3$ generated during the thermal decomposition of HA.

The PSPR value can be reduced to a certain degree by the introduction of the same amount of MBW into the EP matrix. The value recorded for EP2 still reaches 0.46 m^2 s^{-1}. By the presence of 10 phr of MBW@HA, the PSPR value recorded for EP3 lies between the values recorded for the above two composite. The introduction of MBW@HA–DDP into the EP matrix results in a significant decrease in the PSPR value of the composite. It decreases to 0.32 m^2 s^{-1} for EP4. A reduction of 41.8% (compared to the value of pure EP) was observed. Furthermore, the trend in the decrease of the TSP values of the EP composites was similar to the trends in the decrease of the PSPR values when various fillers were added. The lowest TSR value was recorded for EP4. Following the addition of
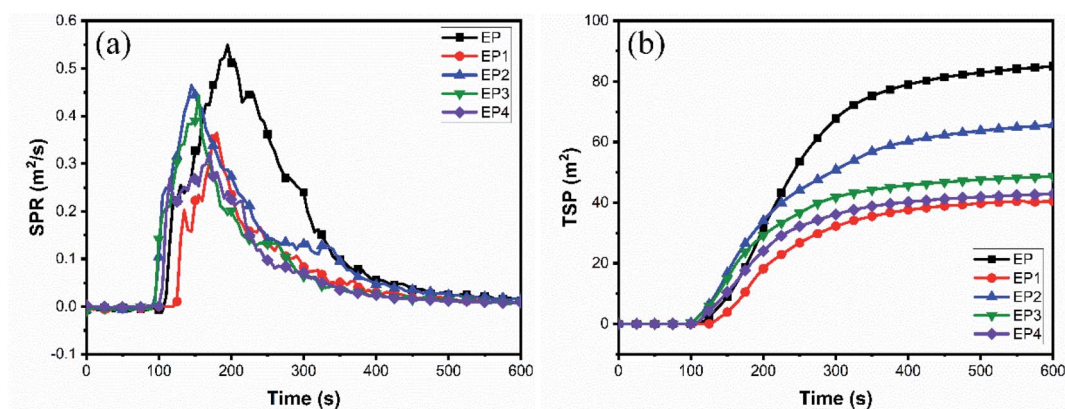

Fig. 7 (a) SPR and (b) TSP curves generated for pure EP and its composites.

MBW@HA–DDP, the value decreased to 43.0 m^2, which is 49.7% lower than the value recorded for pure EP. This can be primarily ascribed to the barrier effect generated by the compact char layer consisting of MBW and the products formed during the thermal decomposition of HA and DDP. The same conclusion was obtained by comparing the thermal degradation behavior of EP and EP composites (the specific results were showed in Fig. S2 and Table S3†).

3.5. Analysis of the char residues formed from EP composites

The char residues formed from pure EP and its composites were investigated to understand the mechanism of generation of the smoke suppression and flame retardancy properties. Fig. 8 presents the digital photos of the char residues. It can be observed that the char residue obtained from pure EP was thin and loose and contained lots of big pores. After the addition of MBW@HA, the damage degree of the char layer for EP3 is

reduced. Nevertheless, there are some white substances piled together without adhesion and cover some surface regions of char surface, which gives rise to the char layer is not continuous. This type of char layer cannot efficiently hinder external oxygen and heat. As to the residue for EP4, it was observed that a compact and continuous char layer was formed following the introduction of MBW@HA–DDP. This char layer can effactually segregate the flammable gases and block the entry of radiant heat and oxygen. Thus, smoke suppression and flame retardancy effects could be increased.

The Raman spectroscopy technique was employed to analyze the components and structure of the char residues. Fig. 9 presents the Raman spectral profiles of the char residues obtained from pure EP, EP3, and EP4. The Raman spectral profile recorded for pure EP exhibits the presence of the characteristic graphitic D band at 1350 cm^{-1} and G band at 1590 cm^{-1}. The bands are associated with the vibrations of the amorphous carbon structure and the ordered graphitic structure,
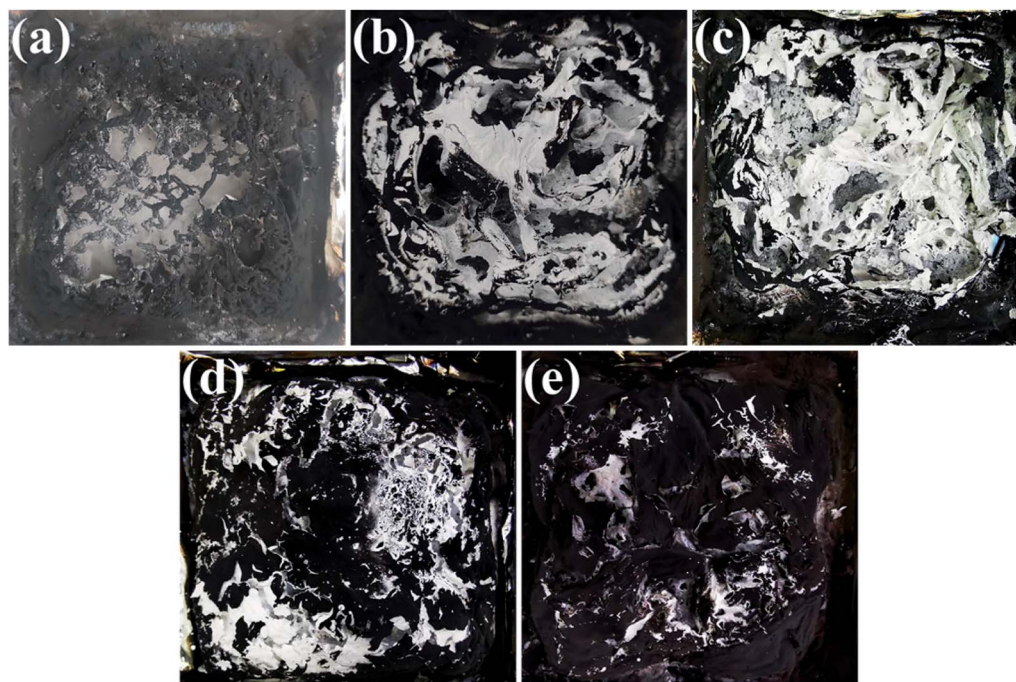

Fig. 8 Digital photos of the char residues of (a) EP, (b) EP1, (c) EP2, (d) EP3, and (e) EP4.
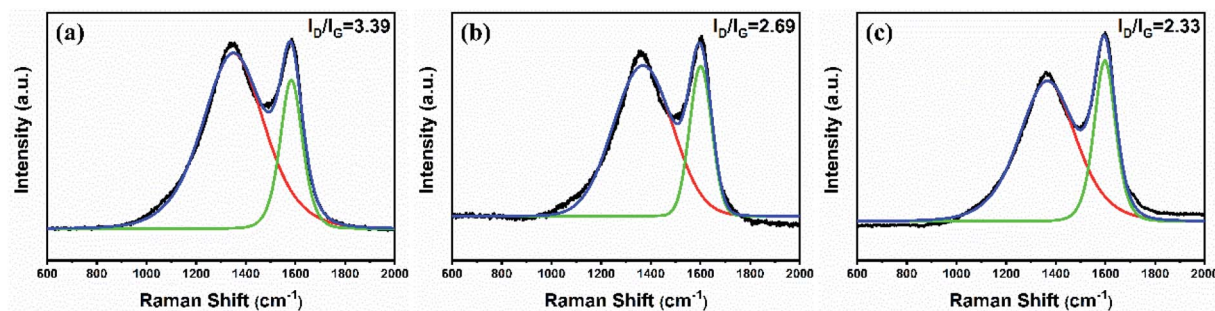

Fig. 9 Raman spectral profiles recorded for the char residue obtained from (a) pure EP, (b) EP3, and (c) EP4.

respectively. The area ratio of the D band to the G band (I_D/I_G) could reflect the degree of graphitization of the char residue. Generally, a lower value of I_D/I_G implies a higher degree of graphitization and the formation of a highly condensed char layer.[44] The spectral profiles recorded for EP3 and EP4 were similar to the spectral profile recorded for pure EP. The I_D/I_G value recorded for pure EP was 3.39. In the presence of 10 phr of MBW@HA, the I_D/I_G value recorded for EP3 decreased to 2.69. This can be primarily attributed to the catalyzing role of Al_2O_3 produced during the decomposition of HA, resulting in the

formation of char. As expected, the I_D/I_G value recorded for EP4 decreased further to 2.33 when the same amount of MBW@HA–DDP was added. This result revealed that the introduction of DDP could improve the extent of the formation of graphitic carbon, resulting in increased compactness of the char layer that blocks the entry of radiant heat and reduces the diffusion of combustible gases.

The XPS technique was also utilized to further investigate the char residues of EP4 collected following CCT. Fig. 10 displays the full-scan XPS spectral profile and the high-resolution XPS
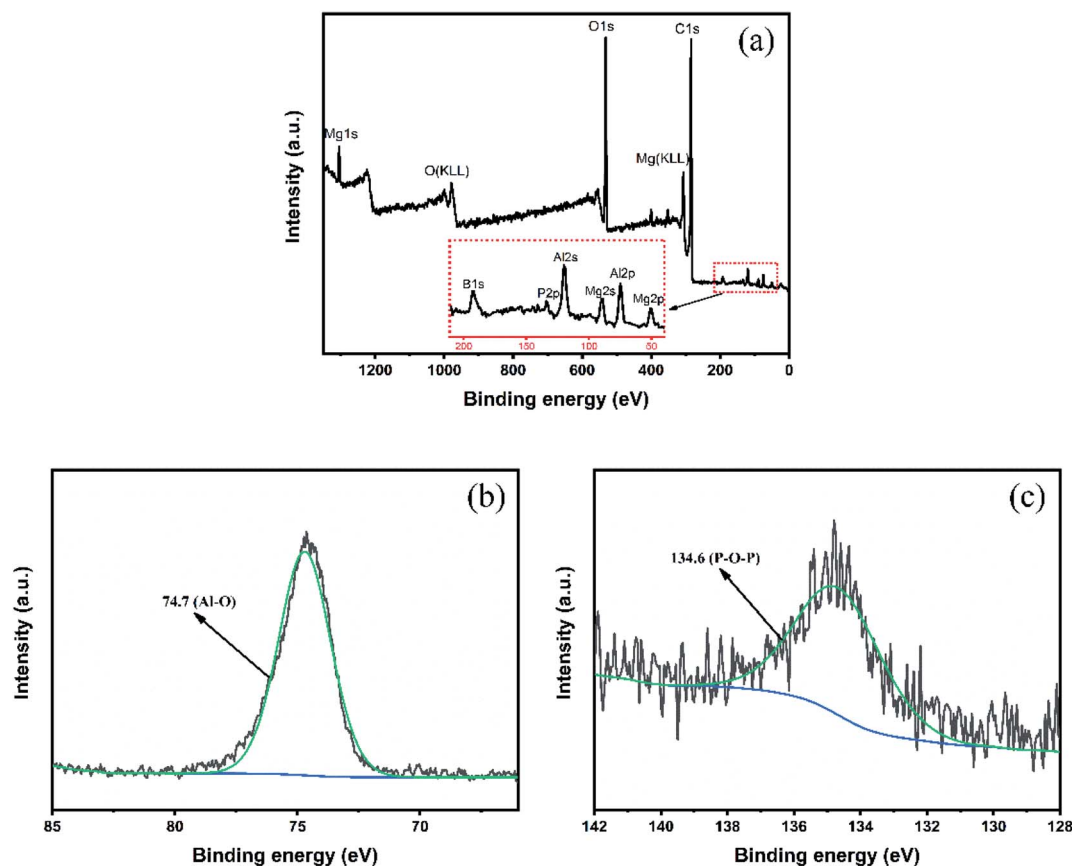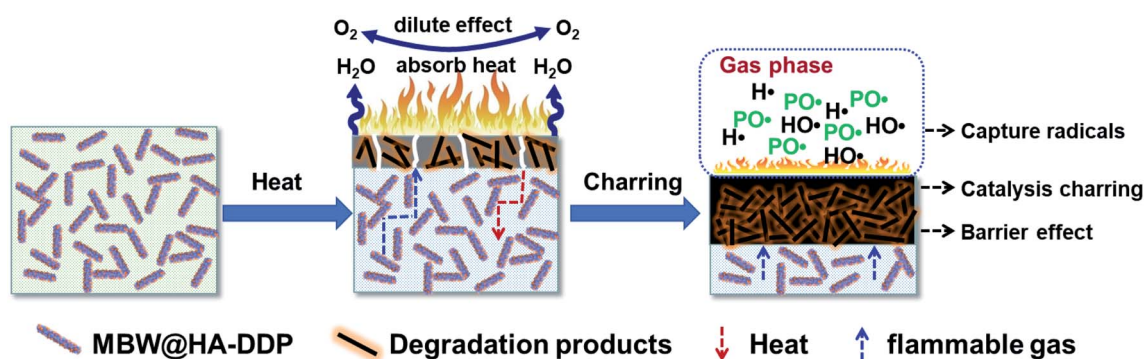

Fig. 10 Full-scan XPS spectral profiles of the char residues formed from (a) EP4 and high-resolution XPS spectral profiles corresponding to (b) Al 2p and (c) P 2p.

Scheme 2 Illustration of flame retardancy and smoke suppression mechanism of MBW@HA–DDP on EP.

spectral profiles recorded for Al 2p and P 2p. Signals corresponding to Mg, B, Al, and P (absent in the profiles recorded for pure EP, shown in Fig. S3†) were detected in the profiles recorded for the char residues of EP4. Meanwhile, analysis of the XRD patterns revealed the presence of $Mg_2B_2O_5$ in the char residue of EP4 (shown in Fig. S4†). Thereby, the peaks for Mg 2p at 50.1 eV and for B 1s at 192.8 eV corresponded to Mg^{2+} and $B_2O_5^{2-}$, respectively. The peak at 74.7 eV could be ascribed to Al 2p of Al–O (Al_2O_3).[39] The binding energy for P2p shifted to 134.6 eV from 133.5 eV (shown in Fig. S5†) following combustion, indicating the breakage of the C–O bond present in P–O–C and the generation of phosphorus oxoacids (phosphoric acid, pyrophosphoric acid, and polymetaphosphate).[45] Based on the analysis above, the plausible mechanism of the generation of the flame retardancy and smoke suppression effect of MBW@HA–DDP on EP is depicted in Scheme 2. The improved fire safety of EP4 could be attributed to the barrier function of $Mg_2B_2O_5$ and Al_2O_3, endothermic effect of HA, dilution effect of water vapor, and process of catalysis of the dehydrated phosphorus oxoacids generated from DDP during the process of combustion.

4. Conclusions

In this study, a novel hybrid containing dodecyl dihydrogen phosphate modified magnesium borate whisker/hydrated alumina (MBW@HA–DDP) was designed and fabricated successfully. The characterization results revealed that the HA flakes could be successfully anchored onto the surface of MBW and DDP could be grafted on their surface. The obtained MBW@HA–DDP was introduced into the EP matrix for the fabrication of EP composites. The results indicated that the incorporation of MBW@HA–DDP could improve the tensile strength and impact strength of EP4 as the strengthening effect of MBW and the degree of interfacial adhesion between MBW@HA–DDP and the EP matrix improved following the introduction of DDP. In addition, the combustion results revealed that MBW@HA–DDP could improve the smoke suppression and flame retardancy ability of EP. The TSP, PSPR, THR, and PHRR values of the EP4 containing 10 phr of MBW@HA–DDP reduced by 49.7%, 41.8%, 28.1%, and 32.0%, respectively, compared to the values recorded for pure EP. The char yield for EP4 increased to 23.4%. The improved fire safety could be ascribed to the barrier function of MBW and HA and the dilution effect of water vapor generated from HA. On the other hand, the phosphorus oxoacids generated from DDP could function as catalysts and increase the degree of graphitization of the char residues. Thus, the introduction of DDP facilitated the formation of char residues and contributed to an improvement in the density of the char layer.

Author contributions

Sai Zou: investigation, writing – original draft. Shengjie Lan: writing – original draft and data curation. Li Dang: formal analysis and methodology. Donghai Zhu: conceptualization, supervision and writing – review & editing. Ping Li: data curation. Le Li: investigation.

Conflicts of interest

There are no conflicts to declare.

Acknowledgements

References

1 X. M. Ye, J. J. Li, W. C. Zhang, Y. T. Pan, R. J. Yang and J. R. Li, *Chem. Eng. J.*, 2021, **425**, 130566.
2 P. F. Qin, D. Q. Yi, J. W. Hao, X. M. Ye, M. Gao and T. L. Song, *Composites, Part B*, 2021, **225**, 109269.
3 S. L. Qiu, C. Ma, X. Wang, X. Zhou, X. M. Feng, R. K. K. Yuen and Y. Hu, *J. Hazard. Mater.*, 2018, **344**, 839–848.
4 W. Peng, S. B. Nie, Y. X. Xu and W. Yang, *Polym. Degrad. Stab.*, 2021, **193**, 109715.
5 M. H. Wang, T. Yu, Z. Y. Feng, J. Sun, X. Y. Gu, H. F. Li, B. Fei and S. Zhang, *Polym. Adv. Technol.*, 2020, **31**, 1340–1348.
6 W. Z. Xu, X. L. Wang, Y. Wu, W. Li and C. Y. Chen, *J. Hazard. Mater.*, 2019, **363**, 138–151.
7 W. W. Zhang, H. J. Wu, W. H. Meng, J. H. Li, Y. M. Cui, J. Z. Xu and H. Q. Qu, *High Perform. Polym.*, 2020, **32**, 359–370.
8 Z. B. Shao, J. Zhang, R. K. Jian, C. C. Sun, X. L. Li and D. Y. Wang, *Composites, Part A*, 2021, **149**, 106529.
9 J. H. Li, Q. L. Wang, M. Li, J. Feng, Z. X. Jia and Y. M. Su, *Mater. Sci.*, 2014, **20**, 289–294.
10 A. Ebdam, S. Jameh-Bozorghi, M. Yousefi and A. Niazi, *Biosci. Biotechnol. Res. Commun.*, 2017, **10**, 54–59.
11 Z. L. Qin, D. H. Li and R. J. Yang, *J. Inorg. Mater.*, 2015, **30**, 1267–1272.
12 M. Baskaran, R. Hashim, J. Y. Leong, Y. N. Ong, M. F. Yhaya and O. Sulaiman, *Bull. Mater. Sci.*, 2019, **42**, 138.
13 M. L. Dong, B. L. Wu, S. D. Xu and P. Hu, *Aust. J. Chem.*, 2018, **71**, 325–333.
14 A. P. Basnayake, J. P. Hidalgo and M. T. Heitzmann, *Constr. Build. Mater.*, 2021, **304**, 124540.
15 A. K. Pathak, M. Borah, A. Gupta, T. Yolcozeki and S. R. Dhakate, *Compos. Sci. Technol.*, 2016, **135**, 28–38.
16 D. K. Rajak, D. D. Pagar, P. L. Menezes and E. Linul, *Polymers*, 2019, **11**, 1667.
17 F. G. Alabtah, E. Mahdi and F. F. Eliyan, *Compos. Struct.*, 2021, **276**, 114595.
18 S. Arulvel, D. M. Reddy, D. D. W. Rufuss and T. Akinaga, *Surf. Interfaces*, 2021, **27**, 101449.
19 I. E. Uflyand and V. I. Irzhak, *J. Polym. Res.*, 2021, **28**, 440.

20 Z. Y. Liu, J. K. Yu, X. N. Wang, L. Zhang, J. K. Wang, E. D. Jin, D. B. Jia, T. P. Wen, Z. G. Yan, L. Yuan and B. Y. Ma, *Ceram. Int.*, 2021, **47**, 30471–30482.

21 Y. Li, J. T. Gao, Z. L. Huang and Z. C. Guo, *Ceram. Int.*, 2019, **45**, 10961–10968.

22 Z. Y. Liu, J. K. Yu, X. N. Wang, X. Zhang, J. K. Wang, D. B. Jia, T. P. Wen, Z. G. Yan, L. Yuan and B. Y. Ma, *J. Australas. Ceram. Soc.*, 2021, **9**, 1298–1309.

23 L. C. Wang, H. H. Wu, S. B. Gao, T. Li, S. Y. Lu, L. Wang and X. P. Huang, *Desalin. Water Treat.*, 2018, **129**, 207–215.

24 O. W. Sheng, C. B. Jin, J. M. Luo, H. D. Yuan, H. Huang, Y. P. Gan, J. Zhang, Y. Xia, C. Liang, W. K. Zhang and X. Y. Tao, *Nano Lett.*, 2018, **18**, 3104–3112.

25 Z. J. Mo, J. P. Chen, J. Lin, Y. Fan, C. Y. Liang, H. S. Wang, X. W. Xu, L. Hu and C. C. Tang, *Chin. Phys. B*, 2014, **23**, 056201.

26 S. H. Chen, S. H. Han, Y. H. Chen, D. P. Xue and X. D. Zhu, *Compos. Interfaces*, 2018, **25**, 1019–1038.

27 J. H. Luo, S. H. Han, J. Wang, H. Liu, X. D. Zhu and S. H. Chen, *Materials*, 2020, **13**, 1698.

28 X. H. Shi, Y. J. Xu, J. W. Long, Q. Zhao, X. M. Ding, L. Chen and Y. Z. Wang, *Chem. Eng. J.*, 2020, **391**, 123584.

29 M. Koyuncu, *J. Trop. For. Sci.*, 2018, **30**, 89–94.

30 P. Khalili, K. Y. Tshai, D. Hui and I. Kong, *Composites, Part B*, 2017, **114**, 101–110.

31 J. Noh, I. Kang, J. Choi, H. Fatima, P. J. Yoo, K. W. Oh and J. Park, *Polym. Bull.*, 2016, **73**, 2855–2866.

32 H. T. Oyama, M. Sekikawa and Y. Ikezawa, *J. Macromol. Sci., Part B: Phys.*, 2011, **50**, 463–483.

33 P. K. Kaul, A. J. Samson, G. T. Selvan, I. Enoch and P. M. Selvakumar, *Appl. Clay Sci.*, 2017, **135**, 234–243.

34 J. P. Long, B. Liang and Z. G. Wang, *Plast., Rubber Compos.*, 2020, **49**, 91–100.

35 K. Y. Li, C. F. Kuan, H. C. Kuan, C. H. Chen, M. Y. Shen, J. M. Yang and C. L. Chiang, *Mater. Chem. Phys.*, 2014, **146**, 354–362.

36 D. H. Zhu, X. Y. Nai, C. C. Zhu, F. Q. Guo, S. J. Bian and W. Li, *Int. J. Miner., Metall. Mater.*, 2012, **19**, 969–972.

37 X. S. Wang, H. C. Pang, W. D. Chen, Y. Lin, L. S. Zong and G. L. Ning, *ACS Appl. Mater. Interfaces*, 2014, **6**, 7223–7235.

38 W. C. Zhu, Q. Zhang, L. Xiang and S. L. Zhu, *Crystengcomm*, 2011, **13**, 1654–1663.

39 Y. S. Zhang, Y. M. Liu, C. Ge, H. B. Yin, M. Ren, A. L. Wang, T. S. Jiang and L. B. Yu, *Powder Technol.*, 2009, **192**, 171–177.

40 Q. H. Zhang and L. Q. Cai, *Pol. J. Environ. Stud.*, 2021, **30**, 2905–2915.

41 L. Dang, X. Y. Nai, Y. P. Dong and W. Li, *RSC Adv.*, 2017, **7**, 21655–21665.

42 W. Z. Xu, B. L. Zhang, X. L. Wang and G. S. Wang, *RSC Adv.*, 2017, **7**, 19662–19673.

43 X. Lu, M. Yu, D. Wang, P. Xiu, C. Xu, A. F. Lee and X. Gu, *Mater. Today Chem.*, 2021, **22**, 100562.

44 W. Z. Xu, B. L. Zhang, X. L. Wang, G. S. Wang and D. Ding, *J. Hazard. Mater.*, 2018, **343**, 364–375.

45 S. Zhou, L. Song, Z. Z. Wang, Y. Hu and W. Y. Xing, *Polym. Degrad. Stab.*, 2008, **93**, 1799–1806.